

Chemical Depth Profiling of Photovoltaic Backsheets after Accelerated Laboratory Weathering

Chiao-Chi Lin, Peter J. Krommenhoek, Stephanie S. Watson, Xiaohong Gu*
Polymeric Materials Group, Engineering Laboratory
National Institute of Standards and Technology, Gaithersburg, MD 20899, USA

ABSTRACT

Polymeric multilayer backsheets provide protection for the backside of photovoltaic (PV) module from the damage of moisture and ultraviolet (UV). Due to the nature of multilayer films, certain material property characterization of a backsheet could only be studied by examining its cross-section parallel to the thickness direction of the film. In this study, commercial PPE (polyethylene terephthalate (PET)/PET/ethylene vinyl acetate (EVA)) backsheet films were aged on the NIST (National Institute of Standards and Technology) SPHERE (Simulated Photodegradation via High Energy Radiant Exposure) with UV irradiance at 170 W/m² (300 nm to 400 nm) under accelerated weathering conditions of 85°C and two relative humidity (R.H.) levels of 5% (low) and 60% (high). Cryo-microtomy was used to obtain cross-sectional PPE samples with a flat surface parallel to the thickness direction, and chemical depth profiling of multilayers was conducted by Raman microscopic mapping. Atomic force microscopy with peak force tapping mode was used complementarily for cross-sectional imaging. The results revealed that the PPE backsheet films were comprised of five main layers, including pigmented-PET, core PET, inner EVA, pigmented-EVA and outer EVA, along with their interfacial regions and two adhesive layers. UV and moisture degradation on the outer pigmented PET layer was clearly observed; while the damage on the core PET layer was less significance, indicating that the outer pigmented PET layer effectively reduced the damage from UV. In high R.H. exposure, both adhesive layers were severely deteriorated. It was found that the EVA layers were susceptible to moisture at elevated temperature, especially for the pigmented-EVA. Based on the results of accelerated weathering, this depth profiling study brings new understanding to the mechanisms of failure observed in polymeric multilayer backsheets during field exposure.

Keywords: photovoltaic, backsheet, polymeric multilayer, Raman imaging, cross-section, accelerated weathering/aging

1. INTRODUCTION

Polymeric packaging materials are key to photovoltaic (PV) module safety, performance, reliability, and durability in field operation.¹ Backsheet, the outermost packaging material on the back side of a PV module that directly adheres to encapsulant, is the first line of back side defense against environmental aging in the field.² Backsheet is a polymeric multilayer laminate system engineered so that each layer has a different purpose such as weatherability, insulation, adhesion promotion, and light reflection. Fluoropolymers are commonly used as the outer-most weather resistance layer of backsheets due to their remarkable chemical and thermal stability, and polyethylene terephthalate (PET) is often used as an insulation layer (usually core layer of backsheet) because of its low cost, low conductivity and high mechanical strength.^{3,4} Moreover, in order to block ultraviolet (UV) from the back side and redirect reflected sunlight (albedo) from the front side of a PV module, white pigments such as titanium dioxide (TiO₂) and barium sulfate (BaSO₄) are widely used in backsheet layers to modify optical properties of polymeric layers. However, the current requirement of > 25 year service life for PV module is a huge challenge to the performance of backsheet. Practical in-field testing results show that significant backsheet failures such as cracking, yellowing and delamination occurred in even less than five-year service.^{2,5-6} For this reason, more in-depth understanding and investigation on polymeric multilayer backsheet degradation are needed.

Previous research efforts have investigated backsheet degradation and failure by studying either individual material components or mini-modules.⁷⁻¹⁰ However, there are limited studies showing degradation correlation between layers in backsheet films and how different aging stresses impact individual layer. Cross-sectional analysis could provide robust information for depth profiling of multilayer system,¹¹⁻¹⁴ hence, it prompted us to carry out the combination of cross-sectioning using cryo-microtomy and Raman microscopic mapping.¹⁵ In this study, a PPE (PET/PET/ethylene vinyl acetate (EVA)) backsheet that is composed of a PET-based outer layer, PET core layer and EVA light reflection and

adhesion promotion layers was selected as a model sample. Raman imaging was performed on the cross-section to study chemical depth profiling of each layer in PPE backsheets before and after accelerated laboratory weathering.

2. EXPERIMENTAL*

2.1 Samples and accelerated laboratory weathering

Commercial free standing PPE backsheets were used as received. Circular specimens having 19 mm in diameter punched from PPE backsheets were mounted on a sample holder for weathering test. The accelerated laboratory weathering was performed in the NIST (National Institute of Standards and Technology) 2-meter diameter integrating sphere-based high intensity UV weathering facility, referred to as SPHERE (Simulated Photodegradation via High Energy Radiant Exposure).¹⁶ Accelerated weathering conditions in the SPHERE environmental testing chambers were 85°C with two different relative humidities (R.H.) of 5% R.H. (low) and 60% R.H. (high). UV irradiance on the PET outer layer side of the sample was approximately 170 W/m² between 300 nm and 400 nm. Sixty-seven consecutive days (d) of weathering was performed in two separate SPHERE environmental testing chambers at low and high relative humidity conditions.

To prepare the cross-section specimens, 3 mm x 4 mm pieces cut from the center of the 19 mm circular sample were embedded in epoxy molding. Cryo-microtoming was carried out on a Leica EM FC7 (Leica Mikrosysteme GmbH) with glass blade for coarse surfacing and then followed with diamond blade for fine surfacing. The cross-section is parallel to film thickness. Care was taken to make sure the microtoming direction does not cross the layers of PPE and followed with backsheets machining direction.

2.2 Raman imaging and atomic force microscopy (AFM)

Raman imaging was performed on a Senterra Raman microscope with motorized XYZ stage controlled by OPUS 7 software (Bruker). The optical setup of the Raman microscope is dispersive and 180° back scattering coupled with a charge-coupled device (CCD) camera for bright field image. An excitation wavelength at 785 nm was provided by a diode laser. The laser power, number of scans and integration time used were in the range of (25 to 50) mW, (1 to 5) scans and (10 to 20) sec, respectively. A 50x metallurgical objective (N.A. 0.75, MPlan, Olympus) was used for mapping so that the spatial resolution and laser spot size were estimated to be 0.5 μm and 2 μm, respectively.¹⁵ Raman mapping images were generated in a user-defined desired area on the sample cross-section with a step size of 2 μm. Separate Raman images were taken from different regions centered at PET outer layer, PET core layer and EVA layers. All mapping was performed under room temperature.

OPUS 7 software was used for further processing of Raman images and spectra. Firstly, Raman mapping images were trimmed for each layer and each material. The layer thickness presented in each trimmed Raman image is smaller than the actual thickness by (4 to 8) μm due to the laser spot size of Raman microscope. Raman images of fluorescence intensity were then exported. To analyze the evolution of certain characteristic bands, baseline correction was carried out using concave rubberband correction function in OPUS 7. Raman Images and spectra of specific band and measuring locations were then exported and analyzed.

*Certain commercial equipment, instruments or materials are identified in this paper in order to specify the experimental procedure adequately. Such identification is not intended to imply recommendation or endorsement by the National Institute of Standards and Technology, nor is it intended to imply that the materials or equipment identified are necessarily the best available for this purpose.

AFM topographical images were acquired by using a Dimension Icon[®] AFM (Bruker) with PeakForce QNM[®] (Quantitative Nanomechanical Property Mapping) based on peak force tapping mode. An antimony doped silicon probe with reflective aluminum back side coating (RTESPA, Bruker) was used. The probe spring constant is 40 N/m with resonant frequency of 300 kHz. Scan sizes of 20 μm x 20 μm to 40 μm x 40 μm with scan speed of 0.5 Hz were performed at ambient conditions.

3. RESULTS AND DISCUSSION

The optical microscope image of the cryo-microtomed cross-section of fresh PPE backsheet is shown in Figure 1. The PPE backsheet films are comprised of five main layers, including PET outer layer, PET core layer, EVA inner layer, pigmented-EVA and another EVA layer, along with two visible adhesive layers between layers of PET outer and PET core, and PET core and EVA inner. The nominal thicknesses for each layer are 55 μm , 126 μm , 25 μm , 50 μm , 25 μm , 6.5 μm , and 8 μm for PET outer, PET core, EVA inner, pigmented-EVA, EVA outer, PET/PET adhesive, and PET/EVA adhesive, respectively. It is worth mentioning that PET outer layer is heavily pigmented, while PET core layer is lightly pigmented.

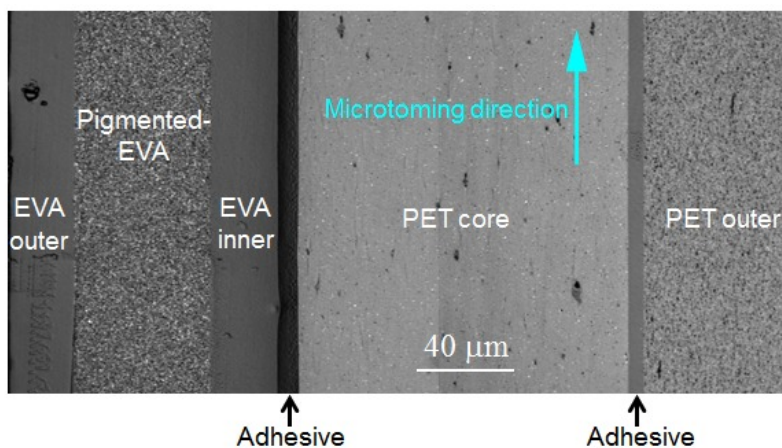


Figure 1. Optical microscope image of the cross-section of fresh PPE backsheet with polymer layers labeled accordingly.

Figure 2 shows raw Raman spectra for each layer of fresh PPE backsheet. For PET layers, as shown in Figure 2(a), the Raman spectra of both PET outer and core layers are quite similar. The main characteristic bands of PET studied are 1726 cm^{-1} , 1614 cm^{-1} , 1115 cm^{-1} , 1094 cm^{-1} , and 998 cm^{-1} due to C=O stretch, ring C=C stretch, mixed mode (ring CH in-plane bend + glycol C-O stretch), mixed mode (ring CH in-plane bend + glycol C-O stretch + COC, CCO bending + C-C stretch), and another mixed mode (glycol C-C stretch + O-CH₂ stretch + ring torsion), respectively.¹⁷⁻¹⁹ Note that the bands in the region of 950 cm^{-1} to 1200 cm^{-1} are correlated with PET conformation and crystallinity,¹⁷ and can later be used as an index to study the depth-dependent degradation. For the PET outer layer, the band at 454 cm^{-1} and the band at 990 cm^{-1} as shown in the inset of Figure 2(a) are due to the white pigment of barium sulfate.^{20,21}

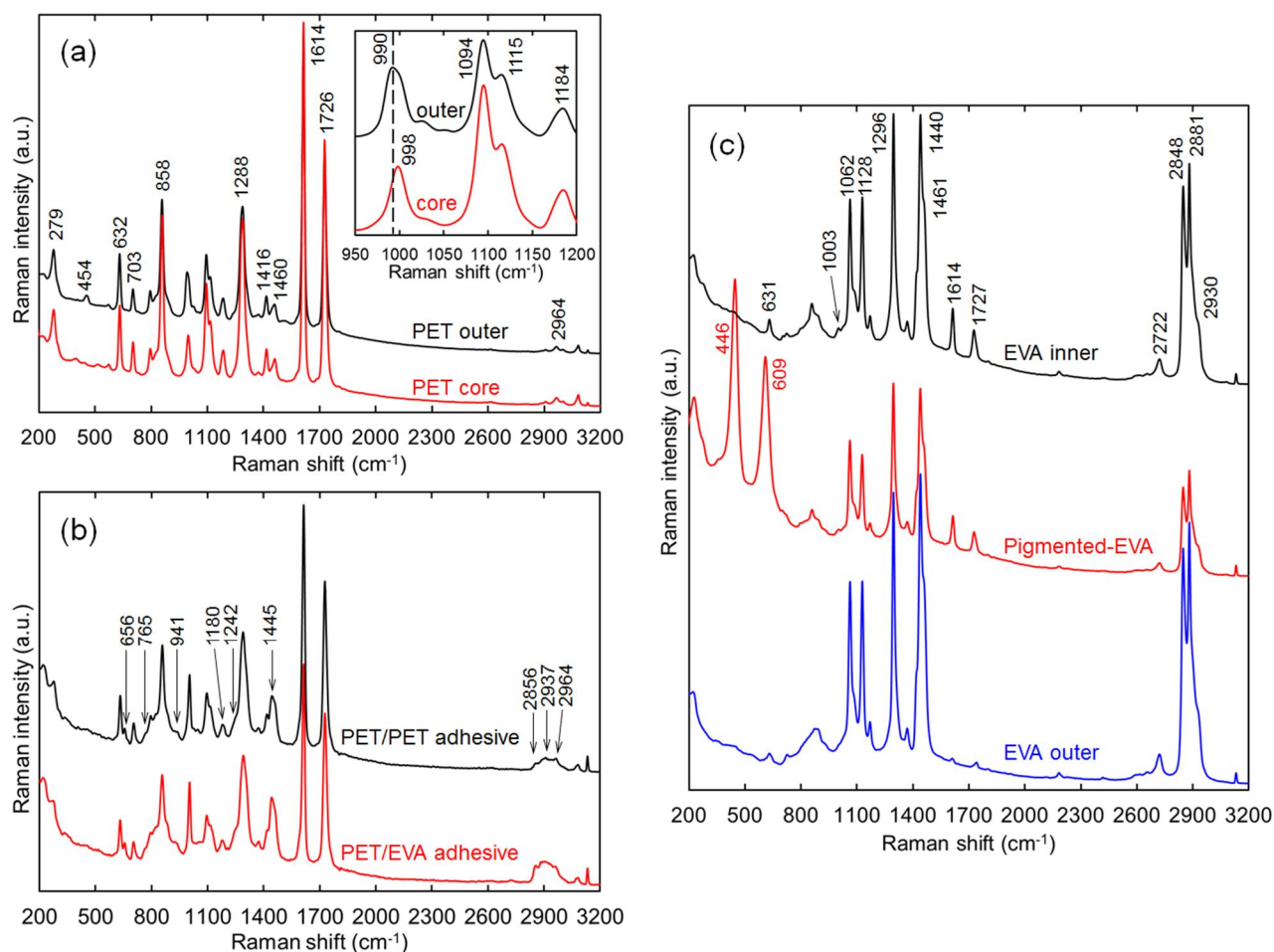


Figure 2. Representative raw Raman stack spectra of (a) PET outer and PET core layers; (b) adhesive layers between PET and PET, and between PET and EVA, and (c) three EVA layers from outer to inner of the cross-section of the fresh PPE backsheet.

Raman spectra of PET/PET and PET/EVA adhesives are shown in Figure 2(b). Both of the Raman spectra are identified as polyurethane due to the distinguished band at 1445 cm⁻¹ and the obvious shoulder at 1242 cm⁻¹ for isocyanate, N-H, and urethane amide III. Based on the characteristic C=O and ring C=C absorptions at 1726 cm⁻¹ and 1614 cm⁻¹, respectively, we suggest that the main composition of the polymer matrix of the adhesives is aromatic polyester-based polyurethane.^{22,23} The characteristic bands at 941 cm⁻¹, 765 cm⁻¹, and 656 cm⁻¹ are the proof of silane coupling agent such as 3-glycidoxypopyl-trimethoxysilane (GPTS) and 3-aminopropyl-triethoxysilane (APTS) in the polymer matrix.²⁴⁻²⁶ Moreover, the P-O band at 1180 cm⁻¹ indicates some phosphorus-oxyacid-based antioxidants were used in the formulation.²⁷ Comparing the aliphatic CH ranges from 2850 cm⁻¹ to 3200 cm⁻¹ between the two spectra, it is believed there were some formulation differences between the PET/PET and PET/EVA adhesives.

EVA layers of PPE backsheet are typical EVA encapsulants as shown in Figure 2(c), and the Raman band assignments have been presented elsewhere.²⁸⁻³³ Note that the bands at 1727 cm⁻¹ and 631 cm⁻¹ are solely from vinyl acetate (VA) of EVA copolymer.²⁸⁻²⁹ Obviously, the EVA outer layer has relatively lower VA content compared with EVA inner layer and pigmented-EVA layer, so that the EVA outer layer is supposed to be an adhesion promotion layer. The pigmented-EVA shows two characteristic bands of the rutile titanium dioxide at 609 cm⁻¹ and 446 cm⁻¹, which is used for enhancing the UV reflection of the film.

In the polymeric multilayer backsheet system, various types of organic additives such as radical-trapping antioxidants, acid resistance agents, hydrolysis stabilizers, heat stabilizers, UV absorbers, antistatic agents, and flame retardants are commonly added in every layer for different purposes. Usually, the amounts of each additive are very small (0.1% to 2% mass fraction), so it is difficult to detect any signal from the additives using conventional vibrational spectroscopy (as shown in Figure 2). However, the photo- and thermal degradation of the EVA, and the interaction between polymeric matrix and additives during accelerated laboratory aging can provide the main contribution of the enhanced fluorescence background to Raman spectra for aged samples.^{10,14,32-33} Therefore, fluorescence intensity can represent overall chemical property and be used as an index to study chemical depth profiling as discussed in the following.

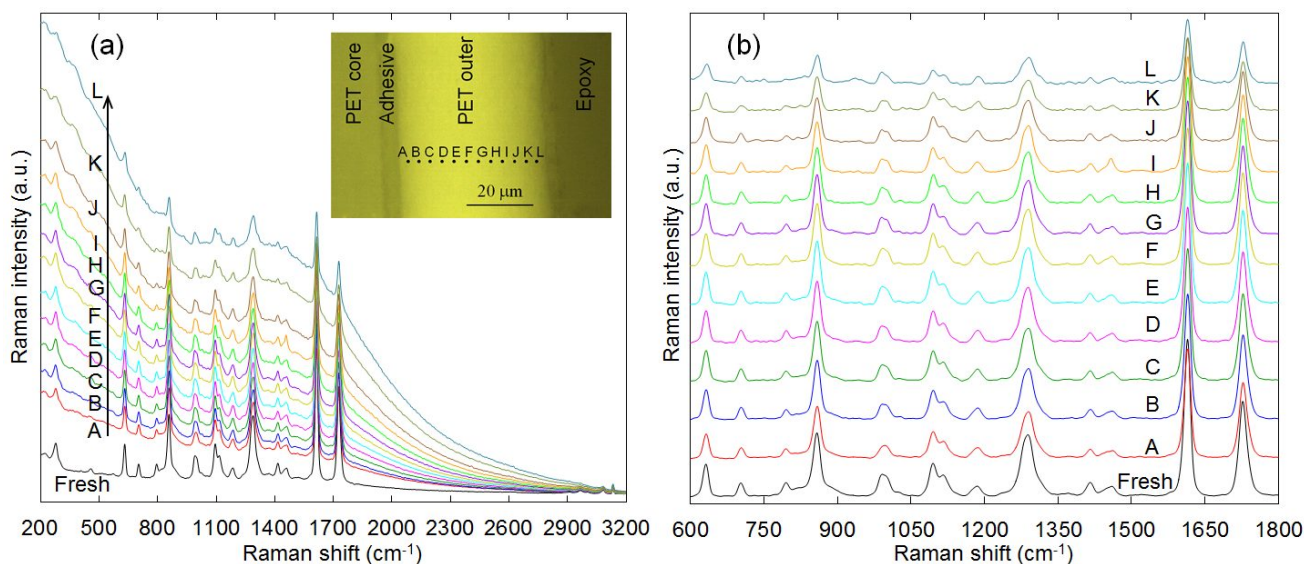


Figure 3. (a) Raw Raman spectra of PET outer layer measured on the cross-section of PPE backsheet after 67 d aging of UV/85°C and 5% R.H. The inset of bright field photomicrograph shows the corresponding measurement locations on the cross-section. (b) The baseline-corrected Raman stack spectra corresponding to the spectra in (a).

An example of Raman mapping spectra, which are the constructing elements of Raman image, is shown in Figure 3. As displayed in Figure 3(a), a set of Raman spectra as a function of depth was exported from Raman image. Each spectrum has its spatial location corresponding to the location on the cross-section (see inset in Fig 3a). The fluorescence intensity evolution as a function of sample depth is obvious; specifically, the closer to the surface of the PET outer, the higher the fluorescence intensity. Raman image based on the fluorescence intensity can be achieved by plotting the integrated area of interest (e.g., 1660 cm^{-1}) in the spectra as a function of an X-Y plane image, as shown in Figure 4(a). On the other hand, for analyses of some specific bands, spectra baseline correction must be performed to eliminate the influence of fluorescence to the band intensity as shown in Figure 3(b). Based on the integrated area of the band of interest in such spectra, the fluorescence-corrected Raman images can be obtained, as shown in Figure 4(b).

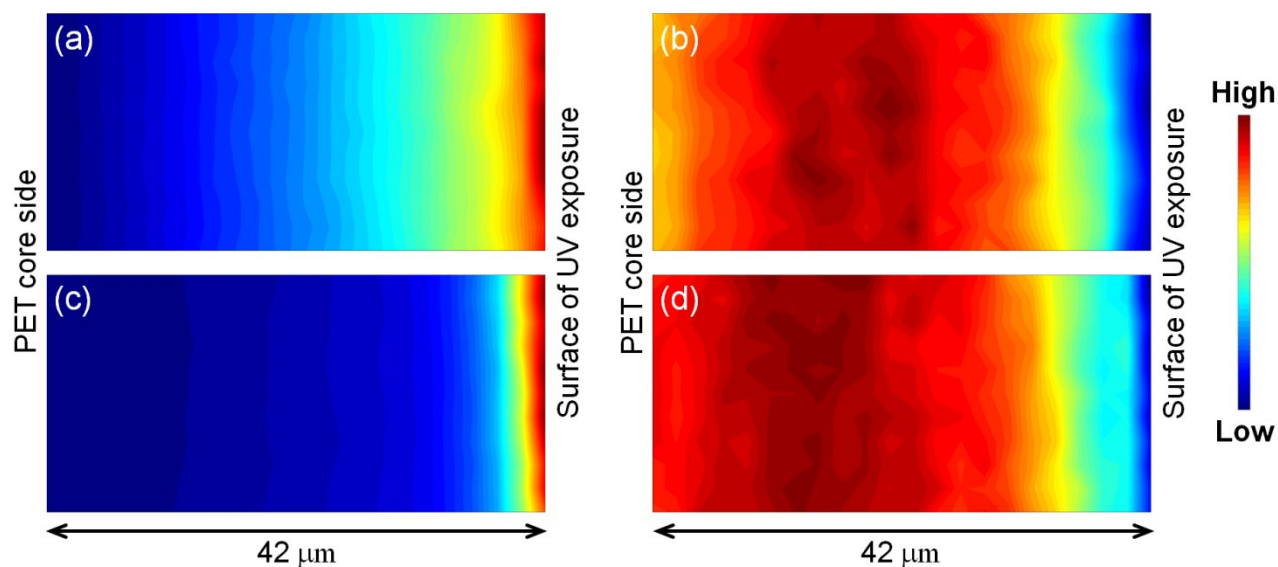


Figure 4. PET outer layer Raman images based on the fluorescence intensity at 1660 cm^{-1} after 67 d aging in UV/ 85°C at 5% R.H. (a), and 60% R.H. (c). Figure 4(b) and 4(d) are the corresponding Raman images (fluorescence-corrected) of C=O band intensity with 5% R.H. and 60% R.H., respectively. All images are normalized to the same intensity of low to high with the UV exposed surface on the right side.

Figure 4 shows Raman images of PET outer layer after 67 d aging in UV/ 85°C at both 5% R.H. and 60% R.H. Figures 4(a) and 4(b) correspond to samples aged at 5% R.H., while 4(c) and 4(d) to those at 60% R.H. The intensity under 1660 cm^{-1} was chosen as an index of fluorescence intensity³²⁻³³ for Raman imaging (Figure 4(a) and 4(c)). The high humidity aged sample presents a sharp change near UV exposed surface, while the low humidity aged sample shows a more gradual change along thickness direction. When using ester C=O band as the main indicator of PET degradation,³⁴ as shown in Figure 4(b) and 4(d), the ester C=O intensity mapping for samples aged at high and low humidities are similar. Note that fluorescence is generated not only by the degradation of PET polymer matrix but also additives such as UV stabilizers, absorbers, and inorganic BaSO_4 pigments. The red region near the surface indicates that the outmost layer of the PPE has the higher fluorescence than the blue central region, which is consistent with the observation of the yellowing on the film surface (yellowing data not shown in this article). On the other hand, the map of C=O band mainly represents the distribution of ester groups remaining in the scanned region after PPE degradation. The blue region near the surface suggests the amount of ester groups in the surface region is lower than those of the central region for the aged PET outer layer, indicating the loss of PET material has occurred during UV exposure.

Furthermore, according to Figure 4, the widths of the PET-deficient region in PET outer layer for both high and low humidity aged PPE are almost same. In other words, the thickness of fresh PET outer layer is $55\text{ }\mu\text{m}$, while the thicknesses of aged PET outer layers are both $42\text{ }\mu\text{m}$ (plus (4 to 8) μm due to laser spot size). That means the depletion of PET due to SPHERE exposure in high and low humidity were similar. For PET crystallinity,^{17,35} based on the intensity of 998 cm^{-1} and the intensity ratio of the bands of 1094 cm^{-1} to 1115 cm^{-1} (Figure 5), the closer to the UV exposed surface, the lower the crystallinity of PET. The results suggest that not only the chemical properties, but also the physical properties have changed after UV exposure. Additionally, in high humidity, distinguished BaSO_4 pigments (990 cm^{-1}) and unknown degradation species ($\approx 1050\text{ cm}^{-1}$) appeared near the UV exposed surface. This may be due to the washing away of the degradation products and further reaction with water (e.g., hydrolysis) for PET. These results are consistent with what was observed in Raman images in Figure 4.

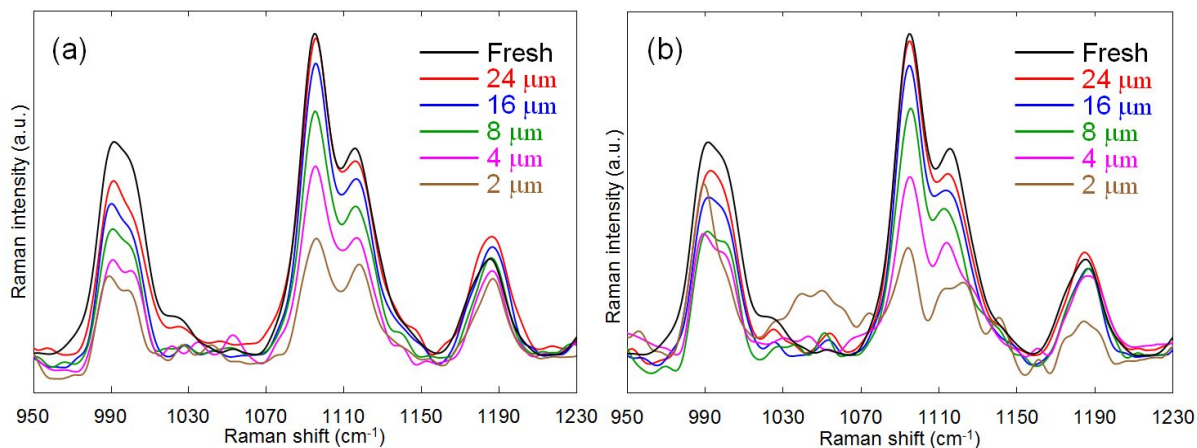


Figure 5. The depth-dependent evolution of Raman spectra of PET outer layer after 67 d aging in UV/85°C, and 5% R.H. (a) and 60% R.H. (b). The UV exposed surface is defined as 0 μm. All spectra here are baseline corrected.

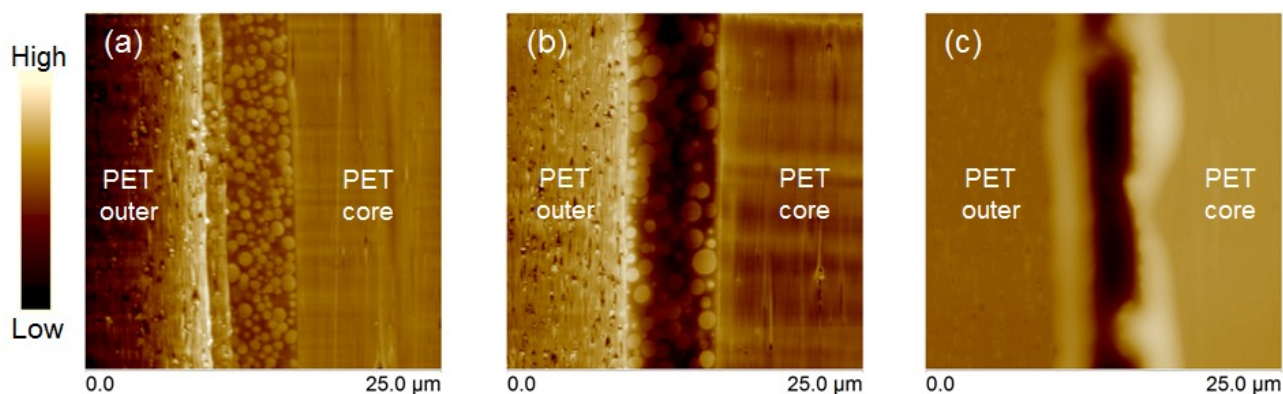


Figure 6. AFM topographic images of PET/PET adhesives, before exposure (a); and after 67 d aging in UV/85°C at 5% R.H. (b), and 60% R.H. (c).

Figure 6 displays the AFM topographical images of the region between PET outer and PET core before and after 67 d exposure on the SPHERE in both low and high humidities. An adhesive layer is clearly observed between PET outer and PET core for the unaged sample (Figure 6(a)), which is consistent with the microscopic images of the same sample shown in Figure 1. The microstructure of this adhesive layer features many small spherical microstructures, similar to the latex structure from emulsion polymerization. After exposure, the adhesive layer became a groove, suggesting that material loss and narrowing have occurred, particularly for the sample aged in high humidity. It was also found that the high humidity-degraded PET/PET adhesive layer was soft and easily smeared. Unfortunately, the high topographic variation in this region made it difficult to acquire meaningful Raman spectra from this area after aging. The topographic changes of this region could be attributed to the further coalescence of those latex-like microstructures (Figure 6(b)), and thermal and hydrolytic degradation of the adhesive layer (Figure 6(c)).

To analyze the Raman mapping data of PET core layer, ester C=O band and fluorescence intensities are chosen to study the degree of the PET degradation. As shown in Figure 7(a) through 7(c), the Raman images based on C=O intensity for aged and unaged samples are overall uniform and similar for different exposure conditions. This result indicates that the PET outer layer effectively block the UV irradiation; otherwise, gradient non-uniformity similar to those observed in Figure 4(b) and 4(d) due to UV degradation of PET would be seen after SPHERE exposure. The random low C=O intensity (blue) spots in the images are caused by the aggregation of pigments as compared with Figure 1. The narrow but distinct blue region near the EVA side as shown in Figure 7(c) indicates the PET degradation in the vicinity of PET

core/EVA inner interfacial region. The map of the fluorescence distribution displayed in Figure 7(d) provides additional evidence illustrating the formation of degradation products with high fluorescence in this interfacial region.

The AFM images in Figure 8 further confirm that more severe changes have occurred in the interfacial region of PET core/EVA inner after SPHERE exposure at elevated temperature and high humidity. As seen in Figure 8(b), for samples aged in low humidity, the PET core/EVA inner region still presented a well-defined interface and nodular microstructures with only minor thickness changes. For those aged in high humidity, substantial changes were observed, and the thickness of the interface was dramatically reduced (Figure 8(c)). Obviously, chemical and topographic changes have occurred in the PET core/EVA inner interfacial region when samples aged in high moisture and elevated temperature, therefore, this is the main reason why moisture damage occurred in PET core layer near EVA side as revealed in Figure 7(c) and 7(d).

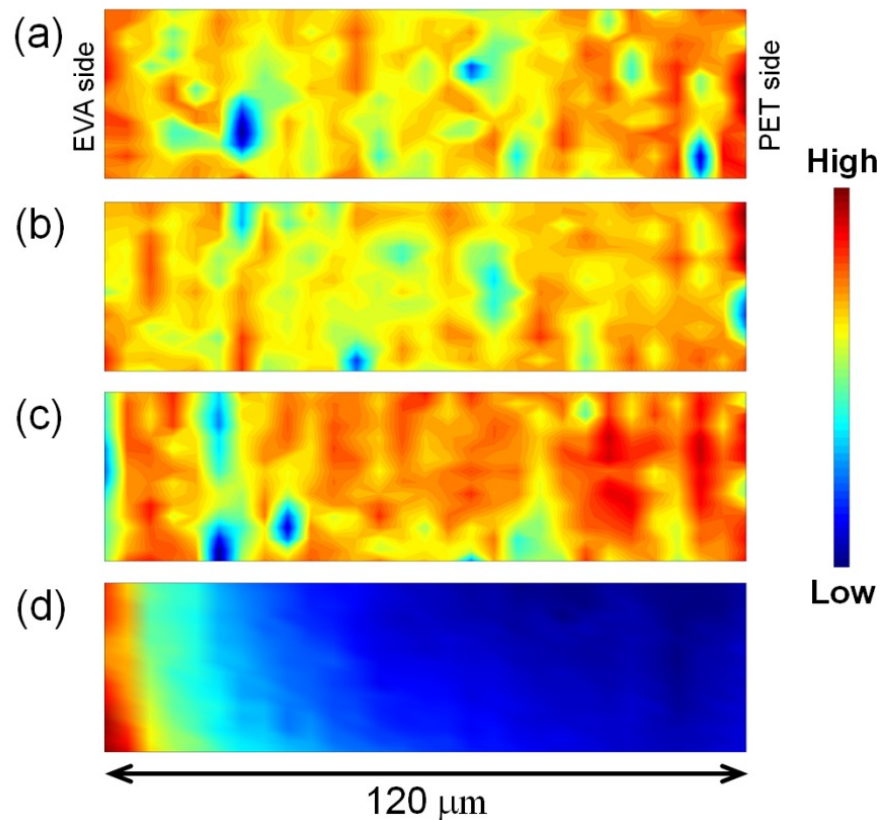


Figure 7. PET core layer Raman images based on the C=O band intensity before (a) and after 67 d aging in UV/85°C at 5% R.H. (b), and 60% R.H. (c). Figure 7(d) is the corresponding Raman image (fluorescence-corrected) of the fluorescence intensity at 1660 cm^{-1} for 60% R.H. aging. All images are normalized to the same intensity of low to high with PET outer layer on the right side.

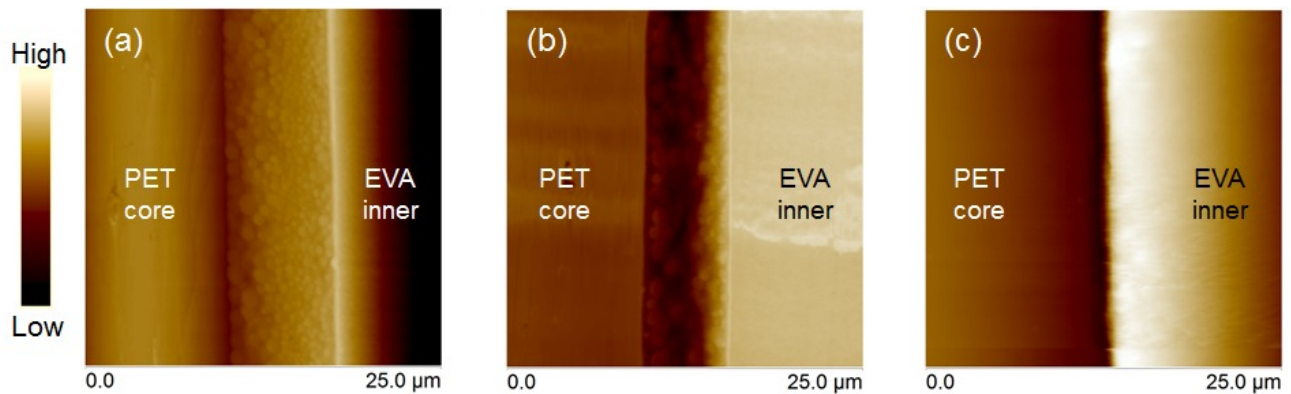


Figure 8. AFM topographic images of PET/EVA adhesives, before exposure (a); after 67 d aging in UV/85°C at 5% R.H. (b), and 60% R.H. (c).

The EVA layers were on the back side of the UV exposure during weathering, but the EVA outer layer was directly exposed to moisture. Because of the low intensity of the C=O band, the aliphatic CH band region around 2800 cm^{-1} to 3000 cm^{-1} was chosen to study the degradation of EVA.^{32,33} As shown in Figures 9(a) through 9(d), the results imply: (1) the lower C-H intensity of the middle pigmented EVA layer in comparison to other EVA layers is probably due to the diluted C-H concentration in the presence of the pigments; (2) the distribution profile of C-H intensity across three EVA layers for the sample aged in the low humidity is similar to that of the fresh sample, only the surface of EVA outer layer has slightly lower C-H intensity, which could be due to chemical degradation of the EVA surface; (3) in high humidity conditions, the thickness of the pigmented-EVA layer is visibly decreased, and the C-H intensity in this layer is lower than the fresh and the low humidity aged samples. Even though these changes could be due to water-assisted degradation of pigmented PET, the detailed mechanism is yet unclear; (4) the vicinity of EVA inner/PET core interfacial region shows a lower C-H intensity, which is consistent with Figures 7 and 8 showing chemical and topographic changes after exposure in high humidity; (5) the strong contrast of Raman image of the fluorescence intensity at 1660 cm^{-1} further confirms that chemical degradation has occurred in pigmented EVA layer during exposure in high humidity. The strong fluorescence indicates that the thermal degradation of the pigmented EVA was probably accelerated with the moisture. This suggests that the degradation in the multilayered structures is not uniform and can be localized.

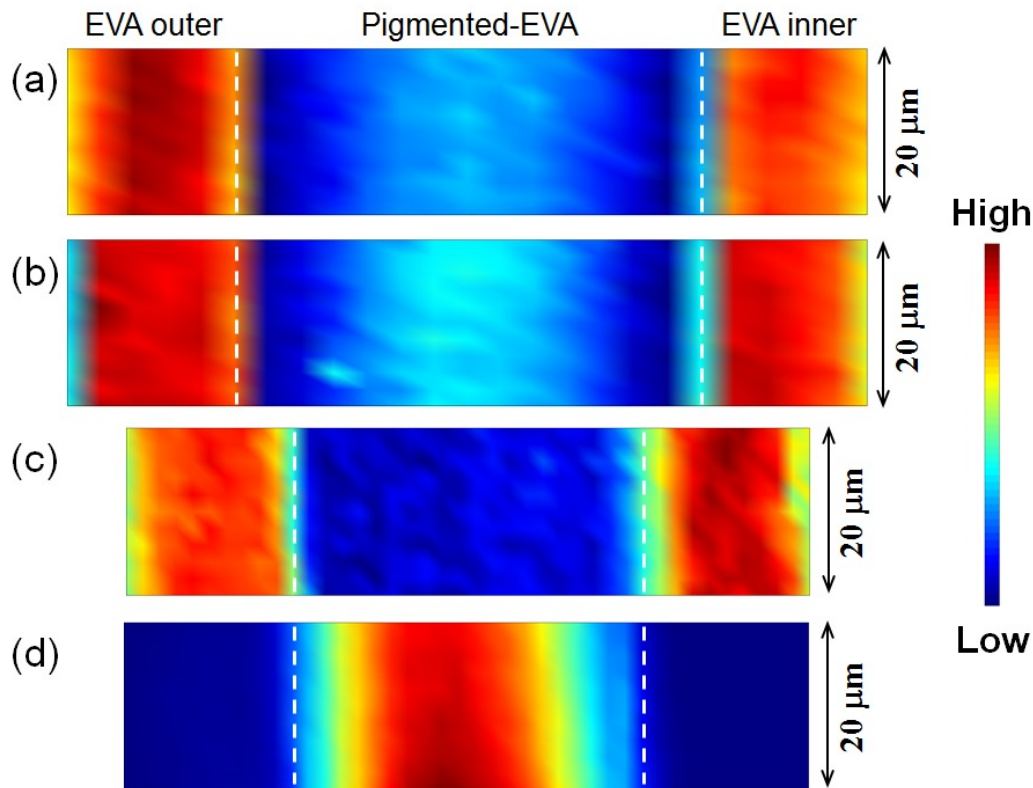


Figure 9. EVA layers Raman images (fluorescence-corrected) based on the aliphatic CH band intensity before (a) and after 67 d aging in UV/85°C at 5% R.H. (b), and 60% R.H. (c). Figure 9(d) is the corresponding Raman image of the fluorescence intensity at 1660 cm^{-1} for 60% R.H. aging. All images are normalized to the same intensity of low to high. The dashed-line in each Raman image represents the interface between layers.

When combining the above data for entire PPE multilayer, results show that when samples exposed to SPHERE with UV, elevated temperature and high humidity, the most susceptible regions are the PPE outer layer, pigmented EVA layer, and the adhesive layers. Besides the UV effect, the humidity also plays an important role in the chemical and structural changes of the backsheets multilayers. Our further mechanical study³⁶ using nanoindentation on the same system is in good agreement and has strongly confirmed the chemical depth profiling observed in this study.

4. CONCLUSIONS

Raman microscopic mapping was used for chemical depth profiling of a commercial PPE cross-sectional sample before and after exposure to NIST SPHERE with UV at 85°C, 5% R.H. and 60% R.H. for 67 d. Based on Raman spectroscopic mapping, it is found that this type of PPE multilayer backsheets is comprised of BaSO_4 -pigmented PET outer layer, PET core layer, EVA inner layer, TiO_2 -pigmented EVA reflection layer, low VA content EVA adhesion promotion layer, and two aromatic polyester-based polyurethane adhesive layers between PET/PET and PET/EVA interfacial regions. Comparing the results of high (60% R.H.) and low (5% R.H.) humidity aging, the pigmented PET outer layer provides acceptable protection for the underneath layers from the damages of UV and moisture. However, the poor moisture resistance of both PET/PET and PET/EVA adhesives, especially the latter, is one of the main weaknesses for failure in the PPE backsheets. Moreover, although EVA is well-known to be susceptible to moisture, the TiO_2 -pigmented-EVA presents more significant chemical and structural changes than the other EVA layers in the high humidity exposure.

5. ACKNOWLEDGEMENTS

This work was conducted with the support of the NIST/industry PV materials consortium. The authors thank all members of this consortium for the helpful discussions. Appreciation is extended to Dr. Lipiin Sung and Dr. Tinh Nguyen at NIST for their discussion and suggestion throughout this work.

REFERENCES

- [1] Jorgensen, G. J., Terwilliger, K. M., DelCueto, J. A., Glick, S. H., Kempe, M. D., Pankow, J. W., Pern, F. J. and McMahon, T. J., "Moisture transport, adhesion, and corrosion protection of PV module packaging materials", *Sol. Energ. Mat. Sol. C.* 90(16), 2739-2775 (2006).
- [2] Gambogi, W., Heta, Y., Hashimoto, K., Kopchick, J., Felder, T., MacMaster, S., Bradley, A., Hamzavytehrany, B., Felix, V., Aoki, T., Stika, K., Garreau-Illes, L. and Trout, T. J., "Weathering and durability of PV backsheets and impact on PV module performance", *Proc. SPIE* 8825, 88250B (2013).
- [3] MacDonald, W. A., Looney, M. K., MacKerron, D., Eveson, R., Adam, R., Hashimoto, K. and Rakos, K., "Latest advances in substrates for flexible electronics", *J. Soc. Inf. Display* 15(12), 1075-1083 (2007).
- [4] Oreski, G. and Wallner, G. M., "Delamination behaviour of multi-layer films for PV encapsulation", *Sol. Energ. Mat. Sol. C.* 89(2-3), 139-151 (2005).
- [5] Ndiaye, A., Charki, A., Kobi, A., Kébé, C. M. F., Ndiaye, P. A. and Sambou, V., "Degradations of silicon photovoltaic modules: A literature review", *Sol. Energy* 96, 140-151 (2013).
- [6] Munoz, M. A., Alonso-García, M. C., Vela, N. and Chenlo, F., "Early degradation of silicon PV modules and guaranty conditions", *Sol. Energy* 85(9), 2264-2274 (2011).
- [7] Wu, D., Zhu, J., Betts, T. R. and Gottschalg, R., "Degradation of interfacial adhesion strength within photovoltaic mini-modules during damp-heat exposure", *Prog. Photovolt.* 22(7), 796-809 (2014).
- [8] Novoa, F. D., Miller, D. C. and Dauskardt, R. H., "Environmental mechanisms of debonding in photovoltaic backsheets", *Sol. Energ. Mat. Sol. C.* 120, 87-93 (2014).
- [9] Kim, N., Kang, H., Hwang, K. J., Han, C., Hong, W. S., Kim, D., Lyu, E. and Kim, H., "Study on the degradation of different types of backsheets used in PV module under accelerated conditions", *Sol. Energ. Mat. Sol. C.* 120, 543-548 (2014).
- [10] Voronko, Y., Chernev, B. S. and Eder, G. C., "Spectroscopic investigations on thin adhesive layers in multi-material laminates", *Appl. Spectrosc.* 68(5), 584-592 (2014).
- [11] Gu, X., Michaels, C. A., Drzal, P. L., Jasmin, J., Martin, D., Nguyen, T. and Martin, J. W., "Probing photodegradation beneath the surface: a depth profiling study of UV-degraded polymeric coatings with microchemical imaging and nanoindentation", *J. Coat. Technol. Res.* 4(4), 389-399 (2007).
- [12] Forster, A. M., Michaels, C. A., Sung, L. and Lucas J., "Modulus and chemical mapping of multilayer coatings", *ACS Appl. Mater. Interfaces* 1(3), 597-603 (2009).
- [13] Adamsons, K., "Chemical depth profiling of multi-layer automotive coating systems", *Prog. Org. Coat.* 45(2-3), 69-81 (2002).
- [14] Planes, E., Yrieix, B., Bas, C. and Flandin, L., "Chemical degradation of the encapsulation system in flexible PV panel as revealed by IR and Raman microscopies", *Sol. Energ. Mat. Sol. C.* 122, 15-23 (2014).
- [15] Zoubir, A., [Raman Imaging], Springer, Verlag Berlin Heidelberg, (2012).
- [16] Chin, J., Byrd, E., Embree, N., Garver, J., Dickens, B., Finn, T. and Martin, J., "Accelerated UV weathering device based on integrating sphere technology", *Rev. Sci. Instrum.* 75(11), 4951-4959 (2004).
- [17] Adar, F. and Noether, H., "Raman microprobe spectra of spin-oriented and drawn filaments of poly(ethylene terephthalate)", *Polymer* 26(13), 1935-1943 (1985).
- [18] Ward, I. M. and Wilding, M. A., "Infra-red and Raman spectra of poly(*m*-methylene terephthalate) polymers", *Polymer* 18(4), 327-335 (1977).
- [19] Lippert, Th., Zimmermann, F. and Wokaun, A., "Surface analysis of excimer-laser-treated polyethylene-terephthalate by surface-enhanced Raman scattering and x-ray photoelectron spectroscopy", *Appl. Spectrosc.* 47(11), 1931-1942 (1993).
- [20] Harroun, S. G., Bergman, J., Jablonski, E. and Brosseau, C. L., "Surface-enhanced Raman spectroscopy analysis of house paint and wallpaper samples from an 18th century historic property", *Analyst* 136, 3453-3460 (2011).

- [21] Srilakshmi, Ch., Widjaja, E., Garland, M. and Anderson, B. G., "Deconvolution of pure component FT-Raman spectra from thermal emission of barium sulfate and graphite samples using the BTEM algorithm", *J. Raman Spectrosc.* 38, 349-355 (2007).
- [22] Parnell, S., Min, K. and Cakmak, M., "Kinetic studies of polyurethane polymerization with Raman spectroscopy", *Polymer* 44(18), 5137-5144 (2003).
- [23] Roohpour, N., Wasikiewicz, J. M., Paul, D., Vadgama, P. and Rehman, I. U., "Synthesis and characterization of enhanced barrier polyurethane for encapsulation of implantable medical devices", *J. Mater. Sci.: Mater. Med.* 20(9), 1803-1814 (2009).
- [24] Riegel, B., Blittersdorf, S., Kiefer, W., Hofacker, S., Müller, M. and Schottner, G., "Kinetic investigations of hydrolysis and condensation of the glycidoxypropyltrimethoxysilane/aminopropyltriethoxy-silane system by means of FT-Raman spectroscopy I", *J. Non-Cryst. Solids* 226(1-2), 76-84 (1998).
- [25] Posset, U., Lankers, M., Kiefer, W., Steins, H. and Schottner, G., "Polarized Raman spectra from some sol-gel precursors and micro-Raman study of one selected copolymer", *Appl. Spectrosc.* 47(10), 1600-1603 (1993).
- [26] Koenig, J. L. and Shih, P. T. K., "Raman studies of the glass fiber-silane-resin interface", *J. Colloid Interf. Sci.* 36(2), 247-253 (1971).
- [27] Trendafilova, N., Georgieva, I., Bauer, G., Varbanov, S. and Dodoff, N., "IR and Raman study of Pt(II) and Pd(II) complexes of amino substituted phosphine oxides: Normal coordinate analysis", *Spectrochim. Acta A* 53(6), 819-828 (1997).
- [28] Shimoyama, M., Maeda, H., Matsukawa, K., Inoue, H., Ninomiya, T. and Ozaki, Y., "Discrimination of ethylene/vinyl acetate copolymers with different composition and prediction of the vinyl acetate content in the copolymers using Fourier-transform Raman spectroscopy and multivariate data analysis", *Vib. Spectrosc.* 14(2), 253-259 (1997).
- [29] Ren, Y., Shimoyama, M., Ninomiya, T., Matsukawa, K., Inoue, H., Noda, I. and Ozaki, Y., "Two-dimensional Fourier transform Raman correlation spectroscopy study of composition-induced structural changes in a series of ethylene/vinyl acetate copolymers", *J. Phys. Chem. B* 103(31), 6475-6483 (1999).
- [30] Macdonald, A. M., Vaughan, A. S. and Wyeth, P., "Application of confocal Raman spectroscopy to thin polymer layers on highly scattering substrates: A case study of synthetic adhesives on historic textiles", *J. Raman Spectrosc.* 36(3), 185-191 (2005).
- [31] Chernev, B. S., Hirschl, C. and Eder, G. C., "Non-destructive determination of ethylene vinyl acetate cross-linking in photovoltaic (PV) modules by Raman spectroscopy", *Appl. Spectrosc.* 67(11), 1296-1301 (2013).
- [32] Peike, C., Kaltenbach, T., Weiß, K. A. and Köhl, M., "Non-destructive degradation analysis of encapsulants in PV modules by Raman spectroscopy", *Sol. Energ. Mat. Sol. C.* 95(7), 1686-1693 (2011).
- [33] Peike, C., Kaltenbach, T., Köhl, M. and Weiß, K. A., "Lateral distribution of the degradation of encapsulants after different damp heat exposure times investigated by Raman spectroscopy", *Proc. SPIE* 7773, 77730E (2010).
- [34] Fehine, G. J. M., Rabello, M. S., Souto Maior, R. M. and Catalani, L. H., "Surface characterization of photodegraded poly(ethylene terephthalate). The effect of ultraviolet absorbers", *Polymer* 45(7), 2303-2308 (2004).
- [35] Štokr, J., Schneider, B., Doskočilová, D., Lövy, J. and Sedláček, P., "Conformational structure of poly(ethylene terephthalate). Infra-red, Raman and n.m.r. spectra", *Polymer* 23(5), 714-721 (1982).
- [36] Krommenhoek, P. J., Lin, C.-C. and Gu, X., "Cross-sectional mechanical and interfacial characterization of photovoltaic backsheets after accelerated laboratory weathering", In preparation, (2014).